Characterisation of Mixing Rate due to High Power Ultrasound

March 20, 2006

Talal F. Yusaf and David R Buttsworth[1]

Faculty of Engineering and Surveying,

University of Southern Queensland,

Toowoomba, 4350, Australia.

email: buttswod@usq.edu.au

Phone: +61 (0)7 4631 2614

Fax: +61 (0)7 4631 2526

[1]corresponding author

Abstract

For meaningful assessment of results from laboratory and pilot plant trials, it is often necessary to know the mixing characteristics within the ultrasonic reactors. Previous workers have used conductivity measurements in an attempt to characterize the residence time distribution in ultrasonic reactors, but these results do not provide direct data on the mixing within the high power region adjacent to the ultrasonic probe tip. We overcome this difficulty though direct visualization of the mixing process within the high energy region close to the tip of the ultrasonic probe. Our analysis proceeds by determining an approximate turbulent diffusivity in a batch reactor arrangement for different values of ultrasonic energy input. For input electrical power levels between 70 and 120 W and a processing volume of 30 ml, the effective turbulent diffusivity varied from about $0.2 \times 10^{-3}\,\mathrm{m}^2/\mathrm{s}$ to $0.7 \times 10^{-3}\,\mathrm{m}^2/\mathrm{s}$. We demonstrate that such results can be coupled to a suitable dispersion model to estimate the actual residence time distribution in flow-though arrangements when the through-put adds little additional mixing energy. Therefore, coupling the effective turbulent diffusivity identified in a batch reactor with a suitable dispersion model for the reactor therefore offers an alternative approach to the deduction of RTD when determining the actual RTD in the high intensity zone of steady flow sonochemical reactors is problematic.

Keywords: ultrasonic processing, turbulent mixing, turbulent diffusivity, mixing time, residence time distribution

1 Introduction

To adequately assess the potential of high power ultrasound in a particular fluid processing application, it is necessary to have some knowledge of the uniformity of the treatment. The flow field established within a high power ultrasound processor has a critical influence on the uniformity of treatment. The intensity of the acoustic field varies with position relative to the ultrasound source [1] and strong acoustic streaming [2] can be established within the processing volume which convects the fluid into or out-of the high intensity treatment regions.

For uniform treatment in a batch reactor arrangement, the characteristic mixing time within the vessel should be small relative to the treatment time. Cadwell and Fogler [3] measured the rate of CO_2 absorption by glycerol in a batch reactor with and without ultrasonic agitation. They related the enhanced absorption with ultrasound to a surface renewal effect associated with the vortex structures they

observed in batch configurations with 20kHz and 800kHz agitation. Vichare et al. [4] analysed conductivity measurements in a sonochemical batch reactor to yield mixing time results for different geometric configurations.

For continuous flow systems, the treatment uniformity (or lack thereof) can be characterized using a residence time distribution, RTD (eg, see [5]). There are many standard techniques for the measurement of RTDs which usually involve introducing a tracer element (such as a saline solution or a dye) at the entrance to the processing device and measuring the concentration of the tracer just downstream of the vessel [5, 6, 7]. Measurements of the RTD in ultrasonic processing configurations have been performed using such tracer methods [8, 9].

In the work of [8], a NaCl tracer pulse was injected into the inlet stream entering their ultrasonic cell. The RTD was identified by monitoring the conductivity within the outlet pipe. Over the tested range of ultrasonic powers and reactor flow rates, the reactor behaved as a continuous stirred-tank reactor (CSTR). Similarly [9] characterised macromixing in their continuous flow ultrasonic reactor by injecting KCl in the inlet and monitoring conductivity in the outlet for different ultrasonic powers and flow rates. In contrast to the arrangement of [8], the configuration of [9] had a characteristic performance between that of a plug flow reactor and a CSTR. For continuous flow arrangements, there are establised methods for estimating an effective turbulent diffusivity or as a nondimensional parameter, the vessel dispersion number, based on an appropriate dispersion model and the measured RTD [5, 6, 7].

However, the introduction of the injection and detection hardware into the system can add a substantial volume which distorts the RTD [9]. Ideally, the actual input to the system should be measured or at least quantified in some manner so that deviations from the ideal impulse or step inputs can be accommodated if necessary through appropriate analysis of the tracer concentration histories [5]. However, even if such measurements are made, the mixing that takes place as the flow enters and leaves the processor can make a significant contribution to the apparent RTD [7]. That is, if significant mixing takes place either side of the important reaction or treatment zone, then it will be difficult to identify the actual mixing that takes place within the treatment zone.

The technique introduced in this paper avoids the difficulties in determining the true RTD by (i) considering the case of an ultrasonic batch reactor arrangement, and (ii) visualizing the mixing process within the high power treatment zone itself. The mixing results are interpreted with the aid of a one dimensional diffusion analysis to yield effective values of turbulent diffusivity. If a geometrically similar continuous

flow configuration is adopted, the effective turbulent diffusivity should remain unchanged at each power level provided the through put of material contributes minimal mixing energy. To confirm this suggestion, we also report an RTD experiment in a geometrically similar continuous flow configuration in which disruption to the basic system due to the injection and detection hardware has been minimised.

2 Apparatus, Methods, and Calibration

2.1 Ultrasonic Processor and Mixing Experiments

The ultrasonic processor was a commercial device (Hielscher UIP500) with a 22 mm diameter probe tip (sonotrode, BS20d22 titanium), operating at a frequency of 20 kHz. The general arrangement of the apparatus used in our experiments is illustrated in Figure 1. Mixing experiments were conducted using a 50 ml Pyrex beaker (internal diameter of approximately 36.5 mm) filled with 30 ml of water and the probe tip immersed to a depth of 7 mm. The water was tap water with no special treatment. The relative position of probe tip within the beaker of water is shown in Figure 2. The probe tip is actually uniform in diameter - the apparent increase in the probe diameter in the submerged regions in Figure 2 is due to refraction. The probe tip is approximately 22 mm from the bottom of the beaker.

With the water stationary in the beaker and the system at a uniform initial temperature of approximately 20 °C, the ultrasonic processor was switch on. After approximately 5 s, a drop of blue food colouring (volume around 0.01 ml) entered the water and proceeded to mix under the agitation of the ultrasonic processor. The mixing process was imaged using a Canon UC-X30Hi 8mm video camcorder and recorded directly onto VHS tape. Mixing sequences were digitised from the VHS recordings using a Pinnacle hard/software and a sequence of around 40 images was saved in jpeg format.

The beaker was back-lit with a 12 V 50 W halogen bulb with DC excitation. The light from the bulb was made somewhat diffuse by placing paper towel between the bulb and the beaker. This relatively high intensity lighting allowed the exposure on the video camera to be manually set to the minimum possible: 1/10,000th of a second. The framing rate remained at the standard 1/25th of a second, but the development of mixing was clearly captured because of the short expose of each frame. The camera iris was also set manually to avoid the camera automatically adjusting the exposure during the experiments.

Five different amplitude level settings on the ultrasonic generator were tested: 26, 40 60, 80, and 100 %.

Note that these values correspond to the markings on the dial of the ultrasonic generator, and these values are not related in a linear manner to the electrical power drawn by the generator or the thermal energy dissipated in mixing volume (see Sections 2.2 and 2.3).

2.2 Input Electrical Power

The electrical power delivered to the ultrasonic generator from the AC mains (∼240 V, ∼50 Hz) was identified by recording the voltage and current signals on a Tektronics digital storage oscilloscope (TDS420A) as illustrated in Figure 1. The voltage and current data was recorded at a sampling rate of 10 kSamples/s giving around 200 samples per AC cycle. Data was transferred to a PC for analysis. The electrical power was identified from

$$P_{elec} = V.I. \tag{1}$$

The instantaneous electrical power delivered to the generator varied through the AC cycle, so results derived from this equation were averaged over the period of each AC cycle. Results from this analysis for three of the five power level settings are shown in Figure 3 for the first few seconds of operation after switch-on.

The electrical power delivered to the generator approaches a steady-state condition after about 1 s of operation. The results in Figure 3 establish that the droplet addition should take place after at least one second of processor operation to ensure steady input of electrical power. Results in Figure 3 are also relevant to the analysis of the thermocouple signals – the first second of operation should be avoided in the calorimetric analysis (Section 2.3) due to the unknown power delivery by the sonotrode during the start-up transients.

Figure 4 shows the variation in electrical power input to the ultrasonic generator with the dial settings. Although the minimum dial setting on the generator was around 26 %, it is certainly not 26 % of the maximum electrical power input under these conditions. The vertical bars associated with each data point in Figure 4 correspond to a variation of ±2 % which is representative of the measured variability associated with manually setting the control dial.

2.3 Thermal Dissipation

To establish the rate of thermal energy dissipation in the water, separate experiments were performed in which a bare wire K-type thermocouple (wire diameter approximately 0.2 mm) was inserted approximately 5 mm from base of the Pyrex beaker, near the centre. The thermocouple signal was amplified using a AD595 chip with the 'cold junction' being formed on the printed circuit board. The voltage signal from the amplifier was recorded using the TDS420A digital storage scope as illustrated in Figure 1.

The thermocouple and amplifier circuit was calibrated using a water bath and a mercury-in-glass thermometer as the reference from approximately 20 °C to 50 °C. Even using this calibration, the absolute temperatures from the thermocouple and amplifier are probably still not accurate to better than 1 °C. However, absolute values of temperature are not required; only temperature changes are of interest for the calorimetric analysis. Thus, for the temperature changes of a few °C that are observed in the experiments, we estimate that the measured temperature changes are accurate to within 5 %.

Calorimetric experiments were performed at the five power level settings (26, 40, 60, 80 and 100 %) and experiments were repeated using different volumes of water (20, 30, 40, and 50 ml) in the Pyrex beaker. A few seconds after processor switch-on, the measured variation of water temperature with time was approximately linear. However, there was some tailing-off of the temperature rise which was noticeable after about 30 s, presumably due to heat loss from the water to the beaker and probe.

The thermal energy that is dissipated by the water can be estimated using the following equation:

$$P_{thermal} = mc\frac{\mathrm{d}T}{\mathrm{d}t} \tag{2}$$

where m is the mass of the water in the beaker, c is the specific heat capacity of the water (taken as 4200 J/kgK for this analysis), and $\mathrm{d}T/\mathrm{d}t$ is the rate of temperature change identified from a linear regression to the data between 5 and 20 s after processor switch-on. The thermal dissipation estimated in this manner for each power level is presented in Figure 5. The horizontal bars associated with each data point represent the ±2 % variability in the manual setting of the generator (as discussed in Section 2.2), and the vertical bars represent the variation in the results for the four different water volumes that were tested. There was no consistent variation in the results across the four water volumes that were used in these experiments. The thermal dissipation indicated in Figure 5 will underestimate the actual thermal dissipation of ultrasonic energy because of heat losses to the beaker and the probe tip. It is difficult

to estimate the likely magnitude of these heat losses because of the unknown heat transfer coefficients around the beaker and, particularly in the high intensity region of the probe tip.

2.4 Image Calibration

The saturation component of the video images was used in the analysis of the mixing process. Figure 6 presents a typical calibration of the saturation component with the dye concentration in normalised scales. The different lines in this figure correspond to different locations within the image for the same variation in dye concentration. The normalisation is such that a concentration of 0.0 indicates no dye, and 1.0 corresponds to the fully-mixed dye concentration. A saturation of 0.0 corresponds to the level when no dye is present and a value of 1.0 corresponds to the fully-mixed dye value. A concentration of 90 % was used to define the mixing time in the subsequent analysis (Section 3) and this corresponds to a normalised saturation of approximately 0.97, Figure 6.

2.5 RTD Experiments

To demonstrate that results from the mixing experiments in the batch reactor arrangement (Section 2.1) can be used to deduce a residence time distribution (RTD) in a similar continuous flow configuration, an additional experiment was performed. The arrangement for this experiment consisted of a processing geometry similar to that of the Pyrex beaker with the addition of inlet and outlet pipes as illustrated in Figure 7.

The flow rate through the system was 4.7 ml/s and the inlet and pipe diameters were 2 mm. The diameter of the processing volume was 37.5 mm and the volume of water in the processing volume was 31.5 ml. The vertical distance from the centre of the inlet pipe to bottom of the processing volume was 28.5 mm.

A droplet of saline was added at the top surface of the water, in a manner similar to that of the dye mixing experiments, and the injection timing was detected with a pair of electrodes positioned between the saline dropper outlet and the surface of the water. The recirculating arrangement was adopted as a convenient way to ensure the water level in the treatment volume remained constant. The volume of the pipework and pump was designed so that saline tracer did not enter through the inlet to the processing volume on the times scales of interest in the determination of the RTD of the ultrasonic processing arrangement. Ice bath cooling of the recirculating water resulted in a steady state operating temperature slightly below

room temperature.

Detection of the saline arrival in the outlet pipe was achieved using a pair of electrodes as illustrated in Figure 7 and the voltage V_{out} was recorded on the Tektronics TDS420A oscilloscope at a sample rate of 1 kSample/s. The electrodes in the outlet pipe were gold plated with a diameter of 1.4 mm and were separated axially by 3.5 mm between centres. The outlet pipe diameter at the location of the electrodes was 3 mm. Calibrations of the detection system indicated that V_{out} varied with saline concentration in a linear manner (estimated maximum error of 5 %) for the present experiment. A thermocouple was positioned in the processing volume near the outlet pipe and both the experiment and the linearity calibration were performed when the system reached the steady state operating temperature of 16.1 °C.

3 Mixing Results and Analysis

Figure 8 presents a sequence of images showing the initial stages of dye mixing for the 26 % setting and the dye injected from the top left as represented in Figure 1. For each power setting, two experiments were performed: one with injection at the top left, the other with injection at the top right. The sequence in Figure 8 illustrates the acoustic streaming commonly observed in ultrasonic experiments. The frame in which the droplet first appears is taken as corresponding with the time of zero seconds.

To identify the mixing time, a specific window within the image was identified as illustrated by the broken line in Figure 2. The rays within this broken line on the image have passed through approximately 50 % of the total liquid volume. Note that refraction effects give the illusion that the rectangular prism represented by the broken line encapsulates more than 50 % of the liquid volume. The central circle in Figure 2 identifies the location of the ray passing through approximately the centre of the total volume of the liquid.

The saturation component at each pixel of each digitized image was normalised using frames taken prior to the droplet addition and images taken after complete mixing was achieved (when there was no further change in the saturation component of each pixel with time). The normalised saturation of each pixel generally varied between 0.0 (corresponding to no dye) and 1.0 (corresponding to the final or fully mixed dye concentration). However, for pixels close to the injection point, transient values larger than 1.0 were registered soon after injection due to the presence of high dye concentrations at these locations and times. Figure 9 presents the variation in normalised saturation averaged over the window identified in

Figure 2 for the two droplet injection locations and the 26 % power setting. The open symbols in this figure indicate the time at which the normalised saturation reaches a value of 0.97, which, according to the calibration (Section 2.4) should correspond to an average concentration of approximately 0.90.

Times to reach an average concentration of 0.90 within the 50 % volume window were identified for the other power levels in the same way and Figure 10 presents these results. The vertical bars in Figure 10 give the time limits identified from the two different experiments (droplet injection at the top left and top right), and the horizontal bars represent the uncertainty in setting the power level (as discussed in Section 2.2). As expected, the higher power levels produce more rapid mixing. Within the range of powers investigated, and given the uncertainties in the experimental data, the linear regression (the broken line in Figure 10) provides a reasonable representation of the data.

4 One Dimensional Diffusion Analysis

The results presented in Figure 10 are sufficient for the characterization of mixing in this particular ultrasonic batch reactor. However, with some additional analysis it should be possible to apply these results to a continuous flow processing arrangement. The way this can be achieved is by first considering the one-dimensional diffusion equation for the dye concentration C,

$$\frac{\partial C}{\partial t} = D\frac{\partial^2 C}{\partial x^2}\,, \tag{3}$$

where x is the distance, t is the time, and D diffusivity. The appropriate boundary conditions for this equation are,

$$\frac{\partial C}{\partial x} = 0 \tag{4}$$

when $x = 0$ (the location nearest the dye injection location), and $x = l$ (the furthermost point from the injection location within the volume). That is, the dye cannot enter or leave the volume during the mixing process ($t > 0$).

If the initial distribution of dye concentration is,

$$C = f(x) \tag{5}$$

at the time the droplet enters the water ($t = 0$), then the solution of Eq. 3 will be given by [10],

$$C(x,t) = \frac{1}{l}\int_0^l f(x')\mathrm{d}x' + \frac{2}{l}\sum_{n=1}^{\infty} \mathrm{e}^{-Dn^2\pi^2 t/l^2} \cos\frac{n\pi x}{l} \int_0^l f(x') \cos\frac{n\pi x'}{l}\mathrm{d}x' \tag{6}$$

Equation 6 is presented graphically in Figure 11 for different positions within the limits of the volume. The concentration in Figure 11 is nondimensional – the normalisation was the same as that adopted in the experiments; the time is likewise a nondimensional parameter, Dt/l^2. The time at which the nondimensional concentration reaches the value of 0.9 is clearly a strong function of position. For example, at a location $x/l = 0.25$, the concentration reaches 0.9 at $Dt/l^2 = 0.00802$ and then overshoots the steady state value, while at $x/l = 0.75$ (further from the point of injection), the concentration does not reach 0.9 until $Dt/l^2 = 0.268$ (beyond the range shown in Figure 11). It is worth noting that Figure 11 indicates the concentration history averaged over the central 50 % of the volume reaches a concentration of 0.9 at $Dt/l^2 = 0.644$ (as indicated by the open symbol) and this is slightly ahead of concentration history at precisely the centre of the volume (compare the solid line with the nearby broken line in Figure 11).

Taking $l = 45$ mm which is the largest distance across the volume, the effective diffusivity can be identified from $D = 0.644l^2/t$ where t is the mixing time to reach a concentration of 0.9 in the identified volume. The results of this analysis are presented in Figure 12. The vertical and horizontal bars correspond directly with those in Figure 10. Again, within the range of powers investigated, and given the uncertainties in the experimental data, the linear regression (the broken line in Figure 12) provides a reasonable representation of the data.

If we were to apply these results to a geometrically similar continuous processing arrangement with the inflow delivered to the cell via a relatively small diameter pipe, then an appropriate dispersion model for estimating the RTD might be either the closed-closed or closed-open model [6] depending on the flow outlet arrangement. For example, in the arrangement used in [9], where the flow enters the cell via a relatively small diameter (3 mm) pipe positioned below the probe tip and passes out of the high intensity region along the probe shank, the appropriate dispersion model is perhaps the closed-open one. The effective diffusivity identified above could be applied directly in such a dispersion model provided the fluid through put does not substantially alter the cell mixing characteristics. Certainly the RTD's

measured by [9] display the requisite elements of such dispersion models. However as mentioned in Section 1, such RTD's may not be a true reflection of the mixing in the high intensity ultrasound region beneath the probe tip because of distortions that arise due to additional mixing in the injection and detection cells.

5 RTD Results

An experiment was performed to validate the claim that the diffusivity identified in the batch mixing arrangement can be used in estimating the RTD of a geometrically similar continuous processing arrangement. The adopted arrangement was described in Section 2.5, and the ultrasonic generator was operated at the lowest power setting. The results from this experiment are presented in Figure 13. Care was taken to ensure that the introduction of the injection and detection systems would have minimal impact on the mixing characteristics of interest. The origin of the time axis in Figure 13 corresponds to the time at which the saline drop entered the water as identified from the injection timing electrodes.

The boundary conditions for the current processing arrangement are best approximated as closed-closed since there will be minimal mixing across the inlet and outlet of the processing volume. In the case of closed-closed boundary conditions, analytical solutions for the governing equation are not available, although graphical representations for certain values of D/uL are presented in many texts (eg, [5, 7]).

The diffusivity for the lowest power setting identified from the mixing experiments and the one dimensional analysis was about $0.22\times10^{-3}\,\mathrm{m}^2/\mathrm{s}$ (Figure 12). For the flow rate of 4.7 ml/s and the volume diameter of 37.5 mm, the average flow speed in the vertical direction was $u = 4.27\,\mathrm{mm/s}$. The vertical distance from the inlet to the outlet pipe was $L = 28.5\,\mathrm{mm}$. Therefore, based on the previously presented mixing results and the current operating conditions, we can estimate the vessel dispersion number for this case as $D/uL = 1.8$.

The comparison between the experimental RTD result and the theoretical simulation using the dispersion equation and closed-closed boundary conditions [7] is shown in Figure 13. For the experimental results, the nondimensional time t/t_m is the actual sampling time t divided by the mean residence time, $t_m = 6.7\,\mathrm{s}$. (The mean residence time was identified from the volume, 31.5 ml divided by the flow rate, 4.7 ml/s). The nondimensional concentration C/C_0 is the instantaneous concentration C divided by the tracer concentration that would appear at the outlet immediately after injection if the mixing were instantaneous

and complete following the droplet entry to the water C_0. The experimental result has been scaled in the vertical direction to match the theoretical results at the nondimensional time $t/t_m = 1$. Such scaling was necessary because, although a calibration was performed on the concentration detection system, there was not sufficient precision in dispensing the saline droplet volume to use the available calibration to accurately determine the C_0.

The agreement of the experiment and simulated results in the vicinity of $t/t_m = 1$ is forced by the adopted scaling, Figure 13. However, we can still point to the value of the maximum in each result (around $C/C_0 = 0.9$ when the noise is smoothed out in the case of the experiment) and its timing (around $t/t_m = 0.1$) to claim a reasonable level of agreement between the experiment and the simulation. There were some slight geometrical differences between the batch and continuous flow arrangement, principally in the vessel diameter and its volume (Sections 2.1 and 2.5. However, the such differences are minor and the results in Figure 13 demonstrate that it is possible to estimate the RTD for a continuous flow system from a geometrically similar batch arrangement when necessary.

6 Conclusions

We have demonstrated a new technique for the identification of mixing characteristics associated with high power ultrasonic treatment at 20 kHz. The mixing rate within the present batch arrangement (30 ml) is a function of the applied ultrasonic power, but the macroscopic mixing is substantially complete within one second for absorbed ultrasonic power levels greater than 40 W (thermal dissipation).

We have demonstrated a method to deduce the effective diffusivity from the mixing time measurements in the batch reactor. In the present work, the effective diffusivity increased with ultrasonic power and ranged from about $0.2 \times 10^{-3}\,\mathrm{m}^2/\mathrm{s}$ to $0.7 \times 10^{-3}\,\mathrm{m}^2/\mathrm{s}$ for input electrical power levels from about 70 to 120 W. We demonstrate that such values of diffusivity may be applied directly in a dispersion model for the RTD in the high intensity region in continuous flow cell arrangements provided the in/out flow does not substantially augment the mixing adjacent to the probe tip. Therefore, coupling the effective turbulent diffusivity identified in a batch reactor with a suitable dispersion model for the reactor therefore offers an alternative approach to the deduction of RTD when determining the actual RTD in the high intensity zone of steady flow sonochemical reactors is problematic.

In continuous flow processing arrangements where the processing region of interest extends only a few

mm beneath the probe tip, or when the processing volume is quite small, the direct visualisation method suggested here may still find application. However, the characteristic mixing times in such configurations at comparable power levels will be shorter than those observed in this work. Thus, higher video framing rates would be required in such applications.

Acknowledgement

This work was conducted with the support of Dairy Australia (previously Dairy Research and Development Corporation) and Australian Cooperative Foods Ltd, trading as Dairy Farmers.

References

[1] B. Pugin, "Qualitative characterization of ultrasound reactors for heterogeneous sonochemistry", *Ultrasonics*, vol. 25, pp. 49–55, 1987.

[2] J. Lighthill, "Acoustic streaming", *Journal of Sound and Vibration*, vol. 61, no. 3, pp. 391–418, 1978.

[3] M. L. Cadwell and H. S. Fogler, "Ultrasonic gas absorption and acoustic streaming observations", *Chemical Engineering Progress Symposium Series*, vol. 67, pp. 124–127, 1971.

[4] N. P. Vichare, P. R. Gogate, V. Y. Dindore, and A. B. Pandit, "Mixing time analysis of a sonochemical reactor", *Ultrasonics Sonochemistry*, vol. 58, no. 1, pp. 23–33, 2001.

[5] O. Levenspiel, *Chemical Reaction Engineering*, John Wiley and Sons, New York, 3rd edition, 1999.

[6] R. W. Missen, C. A. Mims, and B. A. Saville, *Introduction to Chemical Reaction Engineering and Kinetics*, John Wiley and Sons, New York, 1999.

[7] H. S. Fogler, *Elements of Chemical Reaction Engineering*, Prentice Hall, New York, 3rd edition, 1999.

[8] N. Gondrexon, V. Renaudin, C. Petrier, M. Clement, P. Boldo, Y. Gonthier, and A. Bernis, "Experimental study of the hydrodynamic behaviour of a high frequency ultrasonic reactor", *Ultrasonic Sonochemistry*, vol. 5, pp. 1–6, 1998.

[9] H. Monnier, A. M. Wilhelm, and H. Delmas, "Effects of ultrasound on micromixing in flow cell", *Chemical Engineering Science*, vol. 55, pp. 4009–4020, 2000.

[10] H.S. Carslaw and J.C. Jaeger, *Conduction of Heat in Solids*, Oxford University Press, 2nd edition, 1959.

List of Figures

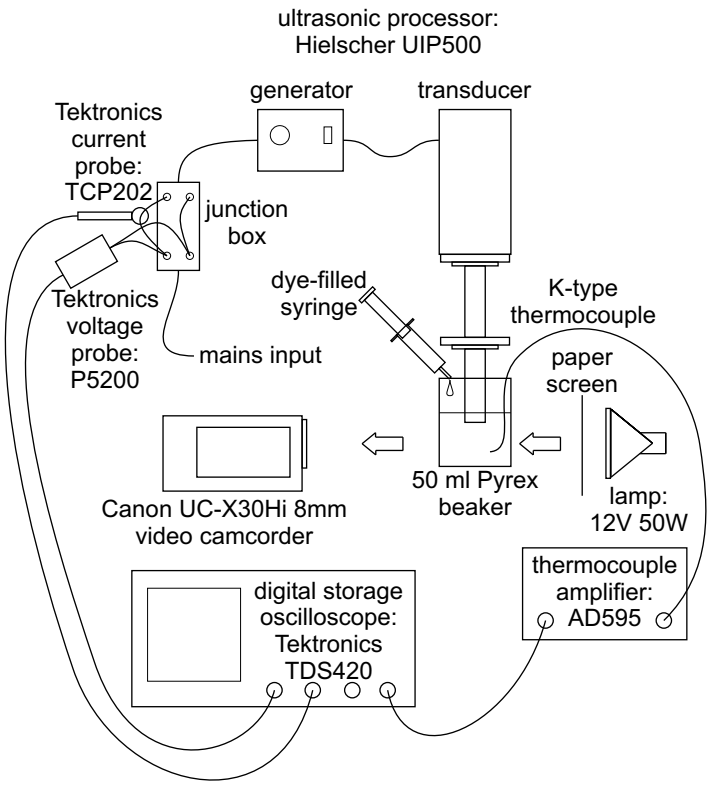

Figure 1: Illustration of apparatus used for electrical power, thermal dissipation, and mixing visualisation experiments.

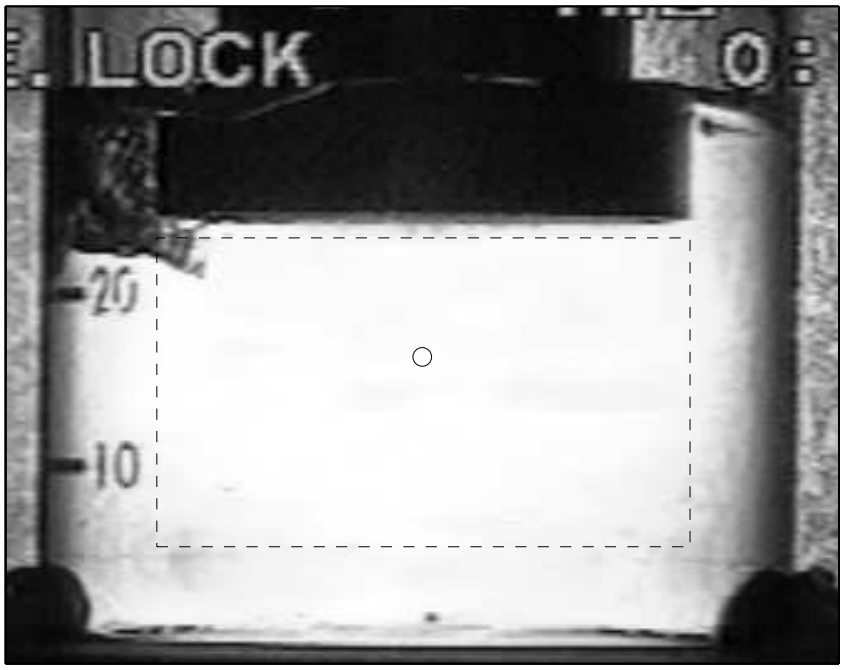

Figure 2: Illustration of the centre of the total volume (the open symbol), and the 50 % total volume region (the broken line) used in analysis. The dye droplet is beginning to spread from the top-left hand corner of the image.

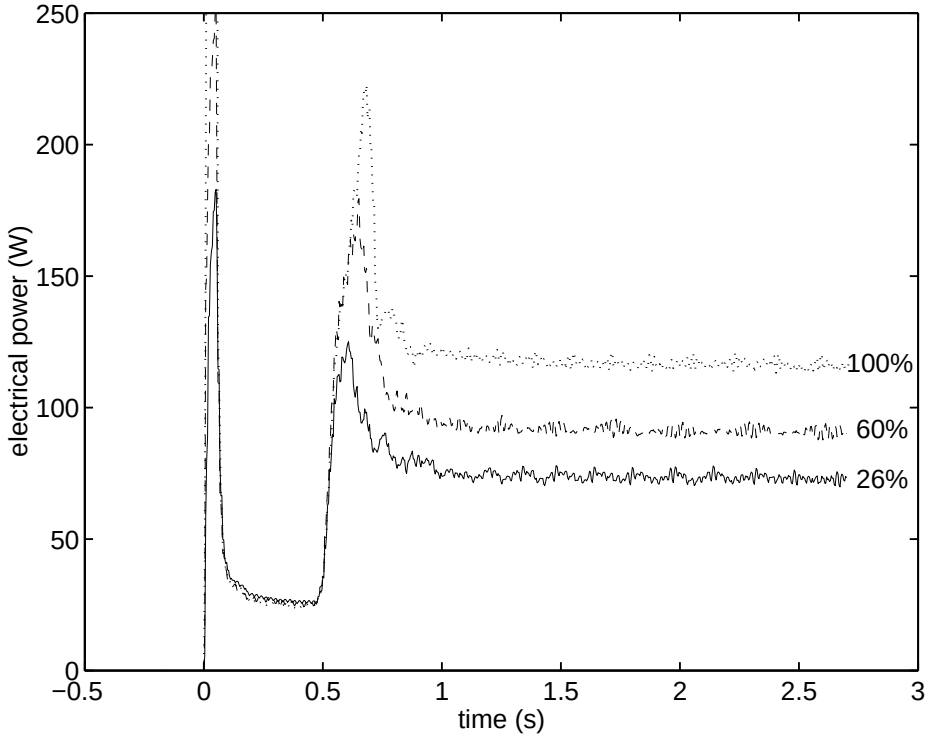

Figure 3: Variation of input electrical power during start-up for three dial settings.

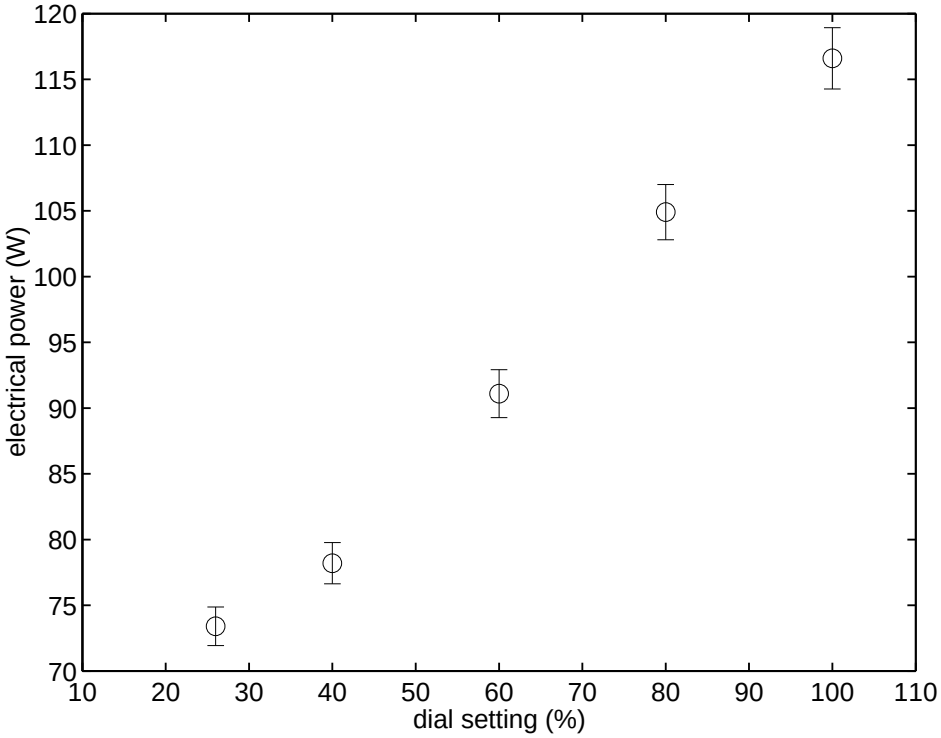

Figure 4: Steady state input electrical power for the five dial settings.

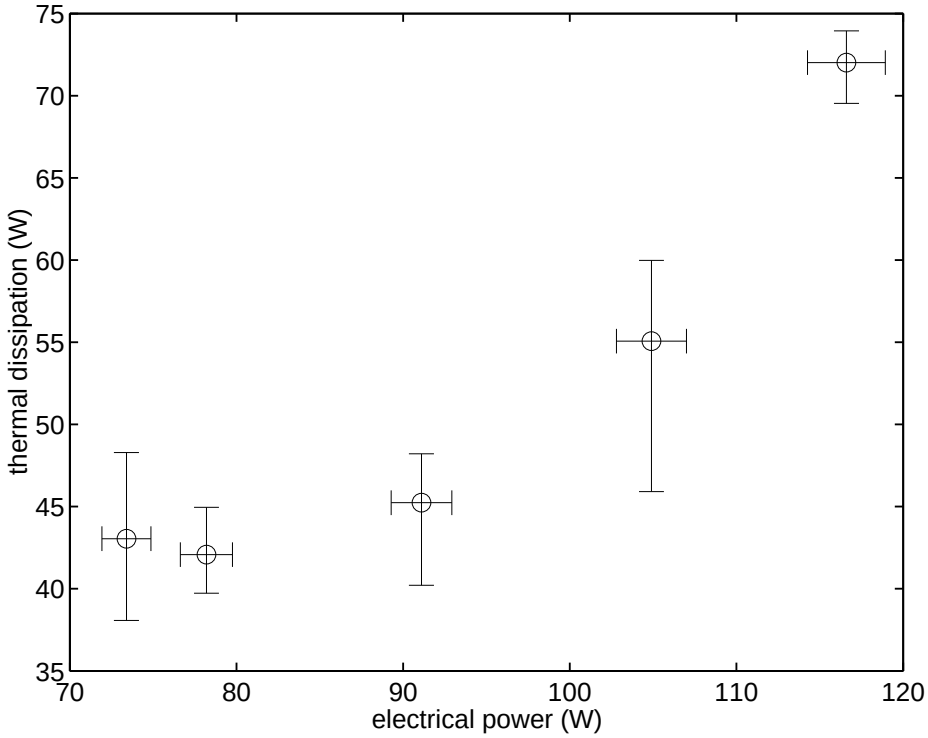

Figure 5: Rate of thermal dissipation for the five levels of input electrical power.

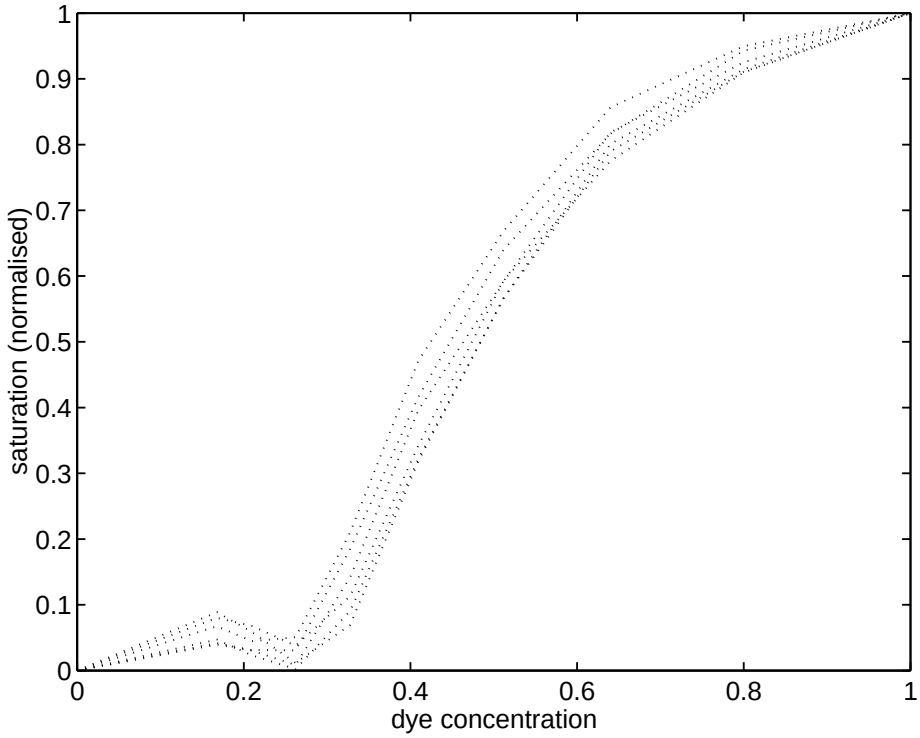

Figure 6: Normalised saturation component of the video image as a function of dye concentration for different positions within the image.

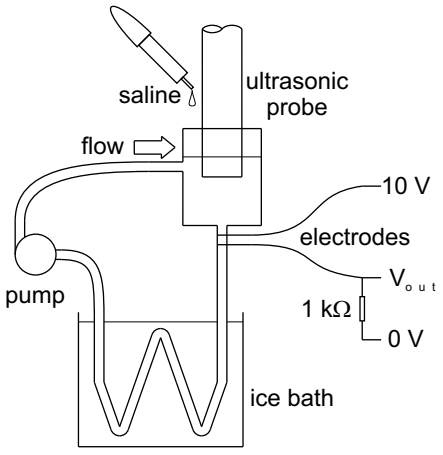

Figure 7: Illustration of arrangement used for RTD experiment.

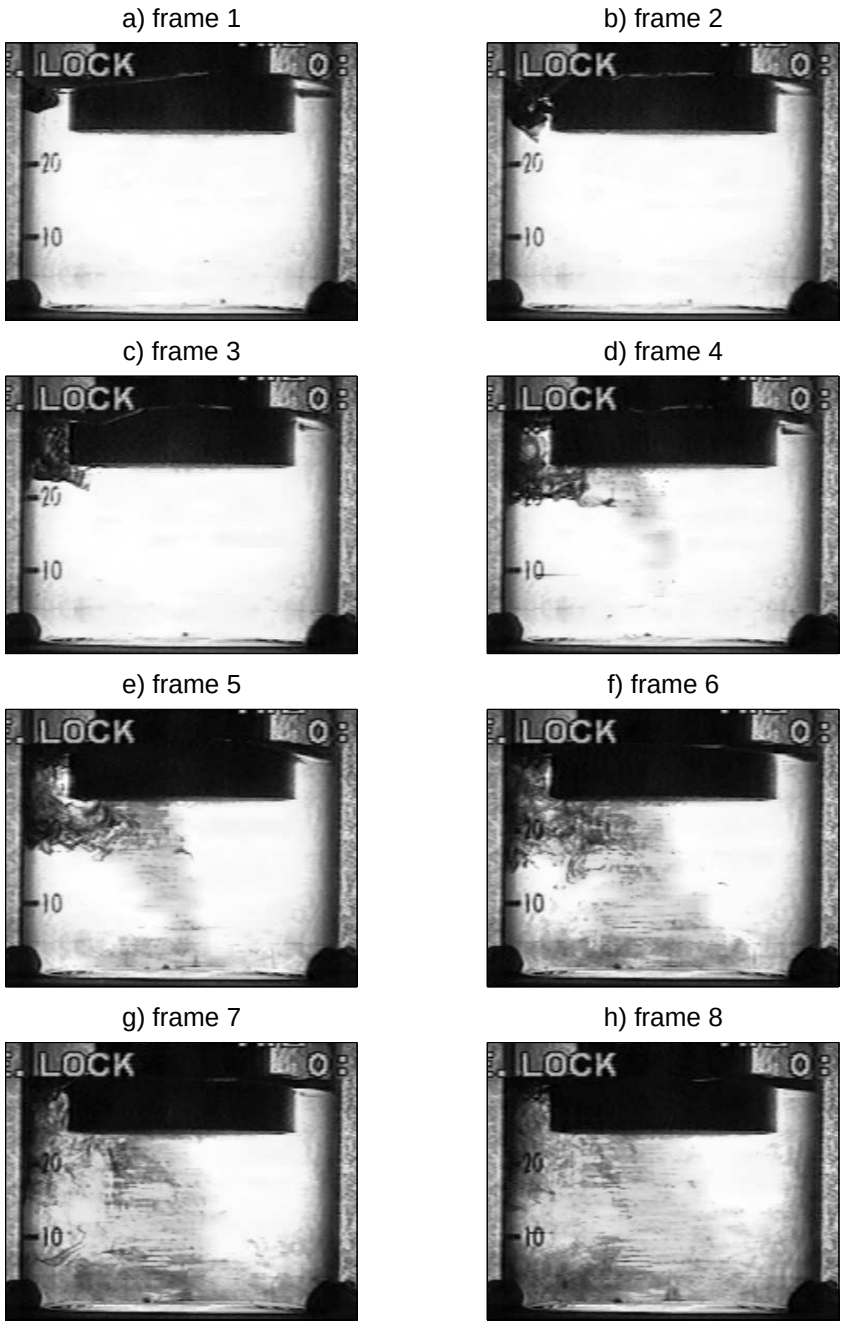

Figure 8: A sequence of video frames showing the development of mixing for the 26 % setting with dye injection on the left. Frame 1, which corresponds to a time of 0 s, shows the dye droplet having just entered the water.

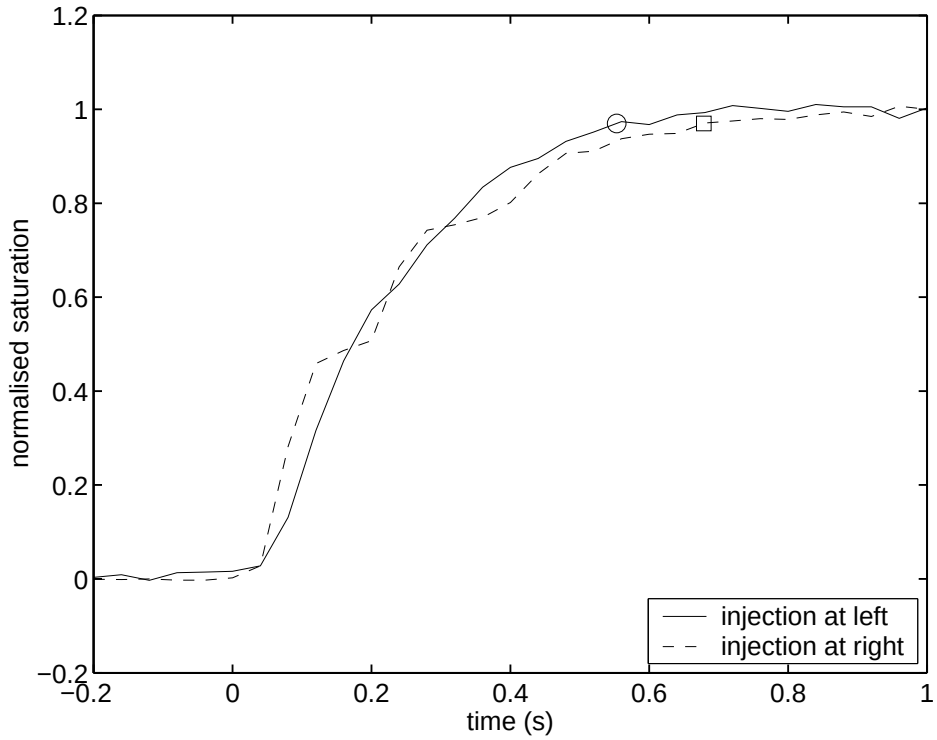

Figure 9: Variation of saturation as a function of time for the 26 % setting for the two different injection positions. The open symbols indicate the time at which the normalised saturation reaches 0.97.

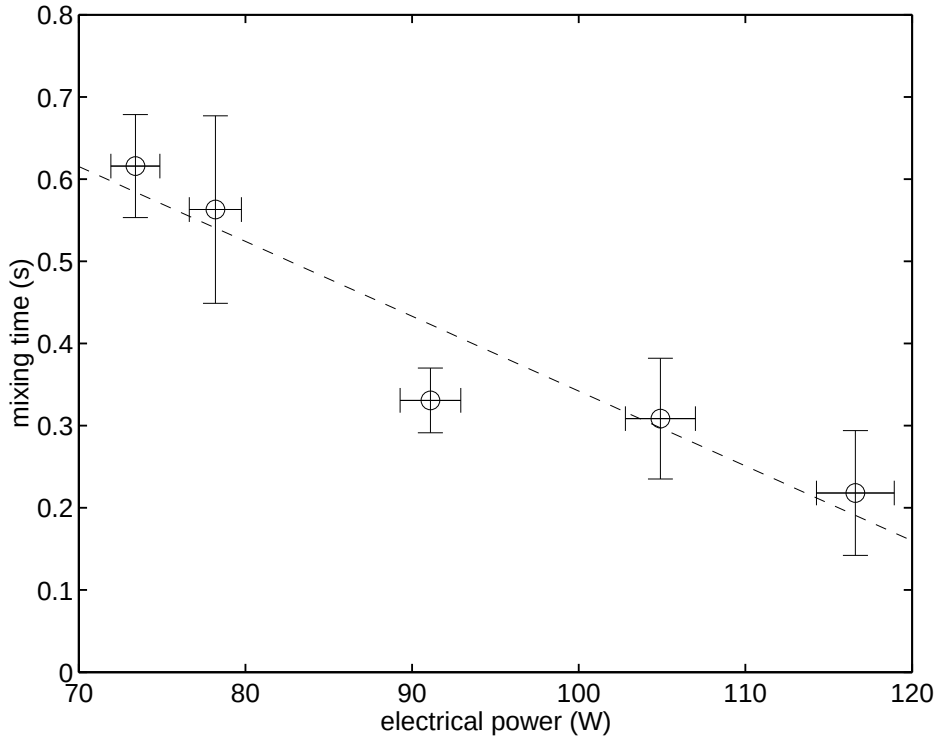

Figure 10: Time to reach a 90 % concentration in the 50 % volume region (the 'mixing time') for the five levels of input electrical power. The broken line represents the linear regression for the data.

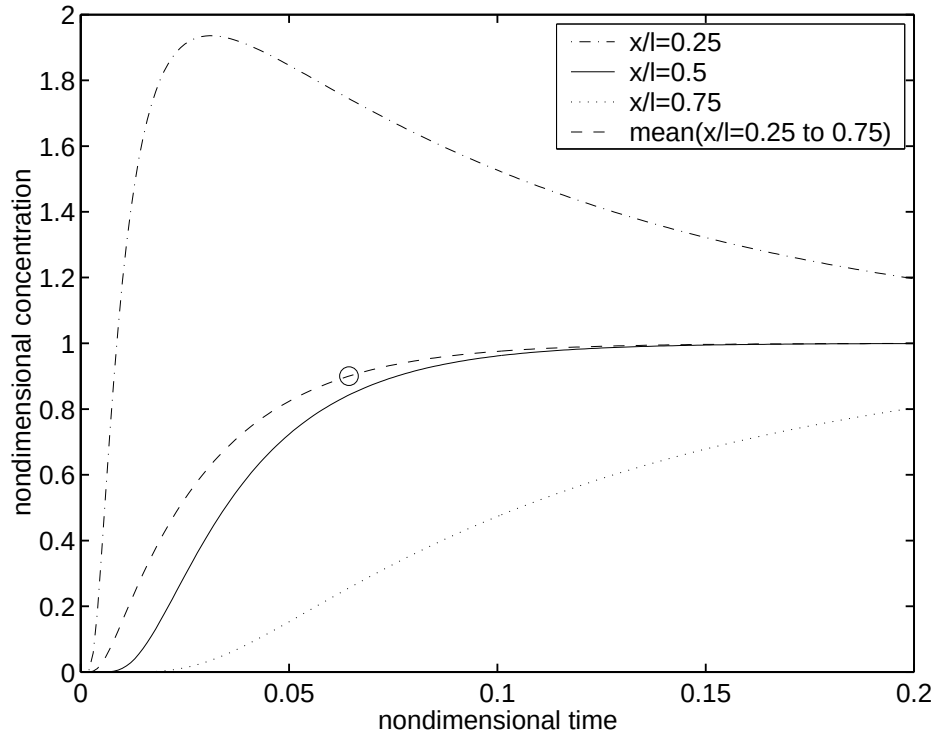

Figure 11: One dimensional diffusion model results. The open symbol indicates the time at which the normalised concentration reaches 0.90 for the centred 50 % volume case.

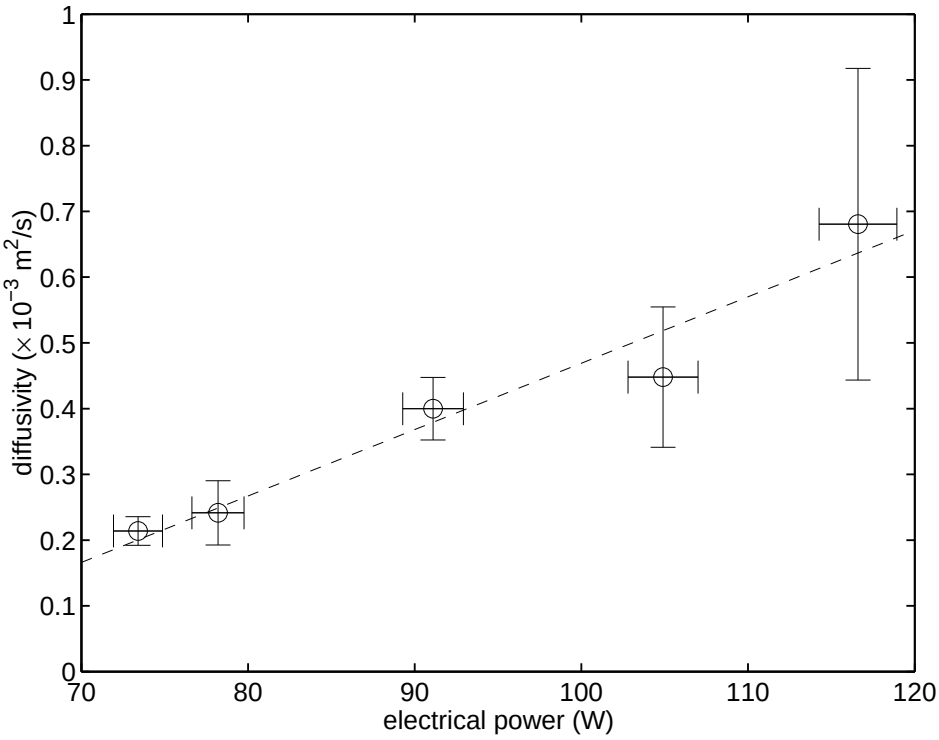

Figure 12: Diffusivity over the range of input electrical powers based on the mixing time data in Figure 10 and the one dimensional diffusion analysis (Figure 11). The broken line represents the linear regression for the data.

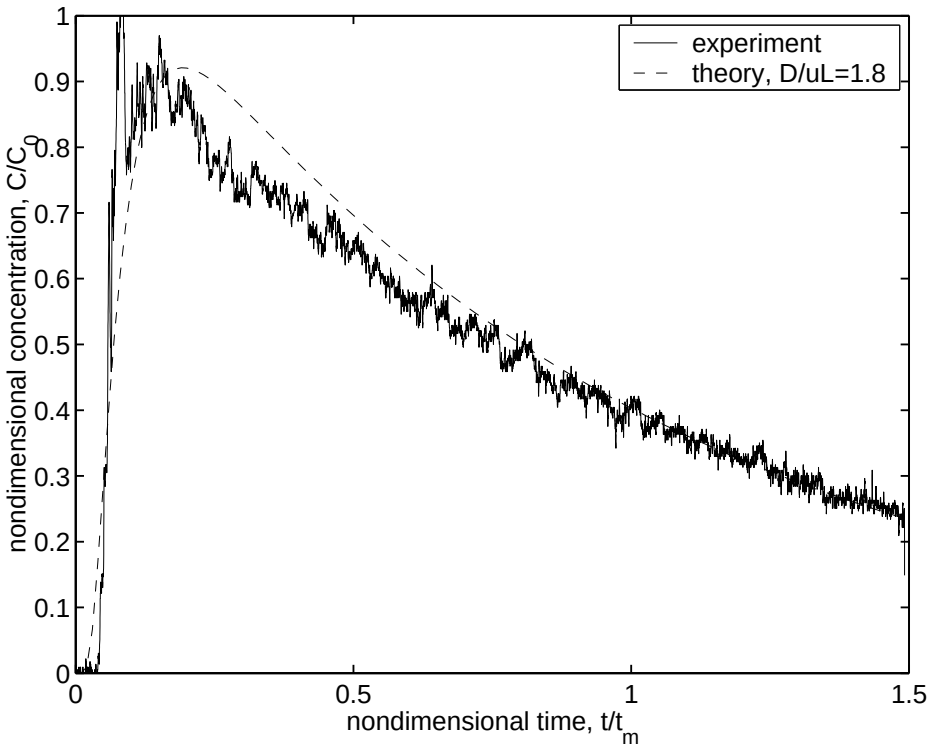

Figure 13: Variation of nondimensional concentration (C/C_0) with nondimensional time (t/t_m) from the RTD experiment and comparison with theoretical curve for $D/uL = 1.8$ and closed-closed boundary conditions.